



Terrestrial laser scanning vs. manual methods for assessing complex forest stand structure: a comparative analysis on plenter forests

Yannik Wardius¹ · Sebastian Hein¹

Received: 27 September 2023 / Revised: 20 November 2023 / Accepted: 30 November 2023 / Published online: 12 January 2024
© The Author(s) 2024

Abstract

In continuous cover forestry, plenter silviculture is regarded as an elaborated system for optimizing the sustainable production of high-quality timber maintaining a constant but heterogeneous canopy. Its complexity necessitates high silvicultural expertise and a detailed assessment of forest stand structural variables. Terrestrial laser scanning (TLS) can offer reliable techniques for long-term tree mapping, volume calculation, and stand variables assessment in complex forest structures. We conducted surveys using both automated TLS and conventional manual methods (CMM) on two plots with contrasting silvicultural regimes within the Black Forest, Germany. Variations in automated tree detection and stand variables were greater between different TLS surveys than with CMM. TLS detected an average of 523 tree stems per hectare, while CMM counted 516. Approximately 9.6% of trees identified with TLS were commission errors, with 6.5% of CMM trees being omitted using TLS. Basal area per hectare was slightly higher in TLS (38.9 m²) than in CMM (38.2 m²). However, CMM recorded a greater standing volume (492.7 m³) than TLS (440.5 m³). The discrepancy in stand volume between methods was primarily due to TLS underestimating tree height, especially for taller trees. DBH bias was minor at 1 cm between methods. Repeated TLS inventories successfully matched an average of 424 tree positions per hectare. While TLS adequately characterizes complex plenter forest structures, we propose enhancing this methodology with personal laser scanning to optimize crown coverage and efficiency and direct volume measurements for increased accuracy of wood volume estimations. Additionally, utilizing 3D point cloud data-derived metrics, such as structural complexity indices, can further enhance plenter forest management.

Keywords Terrestrial laser scanning · Conventional forest inventory · Plenter forest · Continuous cover forest · Automated tree mapping

Abbreviations

ALS	Airborne laser scanning	PCD	3D point cloud data
Automated TLS	Automatic measurements within PCD from TLS	PLS	Personal laser scanning
CCF	Continuous cover forest	RMSE	Root-mean-square error
CMM	Conventional manual method	RSS	Residual sum-of-squares
DBH	Diameter at breast height	Semi-automated TLS	Manual measurements within PCD from TLS
DTM	Digital terrain model	TLS	Terrestrial laser scanning
ICP	Iteratively closest point		

Communicated by Thomas Knoke.

✉ Yannik Wardius
wardius@hs-rottenburg.de

Sebastian Hein
hein@hs-rottenburg.de

¹ University of Applied Forest Sciences, Schadenweilerhof 1, 72108 Rottenburg, Germany

Introduction

Management of plenter forests is traditionally focusing on achieving a continuous yield of tree volume through an ideal forest equilibrium state with a targeted standing growing stock and target tree diameter. Such a state is characterized by a slightly varying distribution across different sized trees, which is mainly determined by the target production goal in tree stem diameter, site conditions, and tree species

composition (Schuetz 2001; O'hara et al. 2007). Compared to other systems of un-even-aged silviculture, a plenter forest is a more specific type of a continuous cover forest (CCF). Plenter forests exhibit a high degree of flexibility, particularly in forest management for timber production. This flexibility is shown in their operational responsiveness to market conditions and forest growth patterns, due to the greater stability inherent in their structure, allowing for quick adaptations of harvesting frequency and intensity (Lenk and Kenk 2007; Knoke 1998; Schuetz 2001). When compared to even-aged forests, plenter forests allow for shorter rotation periods, and application on smaller areas, making them suitable for owners of small forest plots, and easier planning compared to clear-cut forests, when sufficient knowledge on stock and growth is provided. The costs of wood production have also shown to be lower (Zingg et al. 2009). Using principles of thermodynamics, Seidel and Ammer (2023) argue that complex forests, characterized by multiple canopy layers and a diversity of tree ages and sizes, possess greater photosynthetic capabilities which in turn improves thermodynamic processes and consequently increases the forest's adaptability to environmental changes and resilience to environmental stressors. In addition, plenter forests are also expected to be more resilient to wind and snow break than evenly structured forests (Díaz-Yáñez et al. 2017).

Nevertheless, plenter forests reach such advantages due to a very high degree of structural complexity, comprising many classes of tree sizes within a short spatial distance making stand inventories demanding in technical and time resources. As an early method of inventory, the control method (Ger.: "Kontrollmethode") was established in the mid-nineteenth century to monitor this balance (Kurth 1954). However, this conventional form of plenter forest management faces several challenges, including the need for high-quality inventories, silvicultural expertise, and knowledge of forest growth and site properties (Dvorak 2000). This can limit the popularity of plenter forest systems, as seen in Germany where only 2% of the forested land area is managed using plenter forest techniques (Bartsch et al. 2020). Limited knowledge and skills among foresters and forest workers, as well as the lack of resources, were also identified as some of the main obstacles to a widespread adoption of CCF and plenter forest systems in Europe (Mason 2022).

Today, advanced forest inventories, particularly in laser scanning technology, have enabled the use of automated methods to estimate single-tree parameters from three-dimensional point cloud data (PCD). The utilization of airborne laser scanning (ALS) has been adopted by some inventories in Germany, while terrestrial laser scanning (TLS) is nowadays being recognized for its capability to provide detailed insights into the structure and function of

forest ecosystems beyond the limitations of manual methods (Calders et al. 2020; Liang et al. 2016). Conventional plenter forest inventories rely on expensive manual data collection for individual trees, including evaluations of growth, wood volume, and tree stem assessments. Supplementing these inventories with three-dimensional PCD could save time and resources by using automated methods to collect and analyze such data. Basic tree parameters such as tree height, diameter at breast height (DBH), and position can be extracted from the PCD, allowing for the estimation of stem volume and basal area (Hopkinson et al. 2004; Lovell et al. 2003). The traditional method of manual tree growth measurement, using increment drills, can not only be harmful to the probed trees, but also lacks precision (Calders et al. 2020). To overcome these limitations, nondestructive laser scanning methods offer the opportunity for establishing long-term growth and yield plots with accurately mapped and monitored trees and thus calculations of tree volume increment at the individual tree level over time (Ritter et al. 2017).

Our main goal is to examine the feasibility of automated measurement methods using TLS for conducting inventories in highly structured, complex and dense plenter forests. We therefore conducted a survey on selected long-term monitoring plots in a mixed coniferous plenter forest, comparing conventional manual methods (CMM) to automated methods via TLS. Specifically, we aim to compare measurements of individual tree parameters, including DBH, tree height, and stem volume, with stand-level metrics for standing wood volume and basal area. To evaluate the feasibility of establishing a long-term monitoring system of tree growth, we repeated the measurements for each method and compared the rates of successful tree detections as well as the precision and accuracy in determining tree positions and identifying the same trees over time.

Material and methods

Research site

All inventories were conducted in a mixed-species coniferous forest near Loßburg/Freudenstadt County within the Black Forest, state of Baden-Wuerttemberg, Germany. From historical records it is known (Dannecker 1955) that the local forests have been managed according to plenter principles for over 100 years. The study area is located at 750–780 m a.s.l. with a gentle 5° SE-facing slope, as measured on site. We sourced historical climate data between 1970 and 2000 (version released in January 2020) from WorldClim (Fick and Hijmans 2017) with a 30-s resolution, revealing an average annual temperature of 7.1 °C and precipitation of 1593 mm for the research site. The measurements were taken in two

long-term growth and yield plots of 50×100 m each, one named N (no thinning operations over the last 30 years) and the other named H (last thinned in 2007). In 2021, a minor harvest (salvage cutting) was carried out in plot N, removing four trees of 0.24, 0.59, 0.64, and 0.68 m DBH, respectively. The plots were established in 2018 with the following information on site conditions: plot N is strongly acidic, clayey sand, while plot H is a strongly acidic, moderately fresh sandstone soil, according to the monitoring by the Forest Research Station of Baden-Wuerttemberg. The total research area of 1 ha is composed of 78% Silver fir (*Abies alba*), 21% Norway spruce (*Picea abies*), and 1% European beech (*Fagus sylvatica*).

Manual measurements

Both long-term monitoring plots were accurately demarcated according to standard principles of forest growth and yield science (Pretzsch 2009): The coordinates of the four corners of each plot were obtained by repeatedly measuring them with a Garmin handheld GPS device. The location of each tree within the plots was determined by measuring the azimuth and distance from a clearly visible reference point in the landscape nearby. Each tree was numbered, and the DBH ≥ 0.07 m of all trees was measured using a caliper (at 1.3 m stem height). The last available DBH and tree position was recorded in 2022, with previous measurements taken in 2018. Tree height of 40 trees per species and plot, selected to cover the full DBH spectrum, was also available from the 2018 measurement campaign: Three height measurements were taken for each tree, and the mean value obtained from the Vertex IV was finally recorded.

The height of the remaining trees was estimated using the following regression curve proposed by Prodan (2014) for plenter forests:

$$H = 1.3 + \frac{DBH^2}{a_0 + a_1 DBH + a_2 DBH^2}$$

where a_i ($i = 0, 1, 2$) are regression coefficients.

Terrestrial laser scanner measurements

Measurements on both plots using TLS systems were conducted in 2021 using a Leica BLK 360 (BLK) and repeated in 2022 using a higher-end model, the Leica RTC 360 (RTC) with a point measurement rate approximately three times higher than the BLK and a promoted ranging accuracy of 1.9 mm compared to the BLK's 4 mm at a 10-m scanning distance (Table 1). The TLS system was placed along a grid of 10×10 m, aiming to acquire at least 66 scans per plot. With 74 scans on plot N and 71 on plot H for BLK, and 67 for plot N and 70 for plot H for RTC, a few extra scans were necessary to fully capture spots of high tree density, particularly where significant natural regeneration was present. As reference objects, mainly spherical objects with a 0.2-m diameter as well as black and white markers were used attached to a 2-m-tall sighting rod. For processing and registering raw 3D point cloud data (PCD), we used the Leica Cyclone Register. The coordinates of the four measured plot corners were used to georeference the PCD.

3D point cloud data analysis

DBH, tree height and tree position

For the entire processing of the PCD, we used the software R (R Core Team 2023). The analysis was conducted using a consistent R script where only the input PCD files were varied, ensuring a uniform approach in the data processing and analysis stages. After loading the PCD into R, the first step was to filter the PCD based on intensity values. A threshold was set by determining the 90th percentile of the intensity values and only retaining points above this threshold. This way, most of the green vegetation was expected to be removed from the PCD. To normalize the PCD, a digital terrain model (DTM) was created using the k-nearest neighbor (KNN) approach with an inverse-distance weighting (IDW) from the R package LidR (Roussel et al. 2020). Then, the height of all points in the PCD was adjusted relative to

Table 1 Details on point cloud data acquired for this study for each plot (“H” and “N”) and each TLS system used to scan them

Plot	H	N	H	N
Acquisition time	2021, October		2022, October	
Laser scanner	Leica BLK360		Leica RTC360	
Field of view	360° (horizontal)/300° (vertical)		360° (horizontal)/300° (vertical)	
Range	Min. 0.6–up to 60 m		Min. 0.5–up to 130 m	
Point measurement rate	Up to 360,000 pts/sec		Up to 2,000,000 pts/sec	
3D point accuracy	6 mm @ 10 m/8 mm @ 20 m		1.9 mm @ 10 m/2.9 mm @ 20 m	
Scanned area	12,644 m ²	6068 m ²	14,404 m ²	15,148 m ²
Number of points (million)	500.91	500.42	500	500.31
Point density (points/cm ²)	3.96	8.24	3.47	3.3

the ground-derived DTM. Finally, the ground points were removed from the data, resulting in trees placed on a flat surface. In order to identify clusters finally including stems of individual trees, the OPTICS (ordering points to identify the clustering structure, Ankerst et al. 1999) algorithm was applied to the X and Y coordinates to create a reachability plot. After that, clusters were extracted by using the density-based spatial clustering of applications with noise method (DBSCAN, Ester et al. 1996). Clusters with a point count below a specific threshold or an extent under a set height were removed. To remove further points as noise and separate individual objects that were assigned to the same cluster (such as multiple stems within one cluster), the previous process of cluster extraction using OPTICS followed by DBSCAN was repeated for each cluster individually. For this purpose, the algorithms were applied to the X, Y and Z coordinates. Each resulting cluster is expected to contain one individual tree stem. The original PCD includes a 10-m buffer zone around the research plot area. To ensure that the detected tree stems are included in the plot, a polygon was constructed using the four corner points of the plot. By using a point in polygon function, all stems outside the plot boundaries were accurately identified and excluded from further analysis.

The calculation of tree stem DBH was conducted following the approach proposed by Gollob et al. (2020). The tree stems were stratified into 0.15-m-thick overlapping layers, and the Z coordinate of each layer was discarded. The center of each layer was determined by fitting an ellipse to the layer's points. The Cartesian coordinates were then converted to polar coordinates. For each point, the distance and azimuth to the center were calculated. A generalized additive model (GAM) with a smoothing spline was used to model the stem cross section based on the distances and azimuth angles. The diameter of each layer was calculated and subsequently used, along with the layer's height above ground level, in a linear model to predict the diameter at 1.3 m height. The center of the stem cross section at 1.3 m height was also used as the stem's position.

To determine the tree height, a 2-m radius circular clipping area was extracted from the height-normalized original PCD, resulting in a cylinder-shaped section of the PCD. To identify the central tree and remove any non-desired objects, clusters were identified using the OPTICS and DBSCAN algorithms in multiple steps. Non-desired clusters were filtered based on their size and position within the cylinder. Lastly, the height of the tree was estimated as the Z value of the highest point in the remaining cluster. In addition to the automatic measurements within the PCD via automated algorithms, tree height and DBH from PCD were also measured manually. Each clipped tree was loaded into CloudCompare v2.11.3 (CloudCompare Team 2020), where the DBH was calculated using overcross virtual

caliper measurements at roughly 1.3 m height. Tree height was determined by measuring the distance between the stem base and the highest point that, on visual inspection, could be seen as part of the same tree.

Calculating key metrics for forest management

To compare forest stand parameters at the plot level, we calculated a variety of common key metrics frequently used in forest management. These were based on the previously acquired individual tree metrics of tree height and diameter at breast height (DBH). They include standard statistical metrics trees per ha, mean tree height and mean DBH, along with the following:

$$\text{Top Height} = \frac{\sum_{i=1}^n h_i}{n},$$

with h as tree height and $n = 100 \times \left(\frac{\text{Plot area (ha)}}{1 \text{ ha}} \right)$.

$$\text{Basal area (ha)} = \left(\frac{\sum ig(\text{ha})}{\text{Plot area (ha)}} \right),$$

with g as the individual tree cross-sectional area.

$$\text{Standing Wood Volume (ha)} = \left(\frac{\sum_{i=1}^n V_i}{\text{Plot area (ha)}} \right) \times 1 \text{ ha},$$

with V as the individual tree stem volume, determined using the BDAT library in R (Kublin 2003), which is an adaptation of the original Fortran program developed for estimating various tree-related parameters, including volume, employing taper functions. For the volume calculations, tree DBH, height, and species were provided as inputs.

Matching tree IDs from automated TLS—and manual measurements

Both CMM and automated TLS provided the positions for each tree stem on the plot, georeferenced using the WGS 84 coordinate system and UTM zone 32N. In order to monitor individual tree growth over time, CMM can match trees by numbering each stem and thus simply matching a tree by the same number. In order to automatically match trees from PCD, stems were matched based on their position and DBH. To minimize deviations in tree positions, the point datasets containing the tree stem positions for each plot and method of measurement, respectively, were aligned using the iteratively closest point (ICP) search method (Besl and McKay 1992). The ICP algorithm minimizes the distances between the tree stem positions of two datasets from identical plots but different methods of measurement, by iteratively finding a rigid transform that aligns the two-point datasets as closely as possible.

In order to match tree stems, we created a distance matrix between all tree stems of both point datasets, generating a preliminary match based on the closest distance between tree stems. Threshold values were defined to eliminate matches between tree stems with significantly different DBH or positions. After checking for duplicate matches due to missing or unidentified tree stems and deviations in position and DBH estimation, duplicates were eliminated by iteratively looping the algorithm through all duplicate matched tree stems, removing all but the one with the smallest deviation in tree stem position and DBH. Then, the remaining unmatched tree stems were matched with the next candidate from the matrix, which potentially created new duplicates. This process continued until no duplicates or implausible matches remained.

Manual verification of automated measurements

To test the reliability of the automated tree detection, a 2-m-thick horizontal slice of the height-normalized PCD was analyzed for commission and omission errors. For this, the coordinates for each automatically identified tree were imported into CloudCompare v2.11.3 and used to verify whether an object was a tree correctly identified with a DBH equal to or above the 0.07 m threshold, a tree correctly identified but below the said threshold, a non-tree object incorrectly identified as a tree (commission error), or a tree that was not identified at all (omission error). Trees measured during the CMM that could neither be found within the group of correctly identified trees nor among the omitted trees inside the delineated research area were attributed to edge effects. This refers to trees that were excluded due to discrepancies between the physically drawn border and the virtual border within the PCD.

To assess the quality of the automated tree metrics measurements, a circular clipping region from the original PCD, centering on the position of the tree, was imported into CloudCompare v2.11.3 where subsequent measurements for DBH and height were conducted. Although the trees were captured with a TLS and their positions were determined using automated methods, tree metrics were measured manually. Hence, these measurements are termed “semi-automated TLS.”

Results

Tree stem detection, stem position and matching stems

In the 2018 CMM survey of the plenter forest plots, plot N contained 264 trees with a $DBH \geq 0.07$ m, while plot H had 258 trees. During the second manual survey in 2022, a slight

reduction in tree counts was observed. Upon surveying the research site, we confirmed that this was largely influenced by minor harvest interventions and tree mortality.

Automated TLS identified 2.7% more trees from PCD compared to CMM. PCD generated with the BLK detected 17.4% more trees within the survey areas than those obtained with the RTC. On average, 9.6% of the tree stems identified using automated TLS are considered commission errors, whereas 6.5% of trees were omitted. Only the smallest fraction of the commission errors was composed of non-tree objects. The impact of commission errors was more prominent in PCD by the BLK model compared to the RTC model, which had a higher rate of omission errors. The distribution of detection outcomes comprising commission errors, omission errors, and correct detections is illustrated in Fig. 1, complemented by corresponding descriptive statistics in Table 2.

On average, a corresponding tree from CMM was found for 80% ($\sigma = 8.5\%$) of all trees identified from PCD by automated matching of trees. Conversely, 81% ($\sigma = 7.3\%$) of the trees measured by CMM were subsequently identified automatically in the PCD. Repeated measurements using the two different TLS models led to a match of 212 trees on average, which equals 87% of the trees detected by the RTC and 74% of the trees using the Leica BLK (Fig. 2).

Trees identified from PCD, which could not be matched with those from CMM, were found to be overrepresented near the borders of the survey plots. 25% of these unmatched trees, as identified from PCD, were situated 1.86 m or closer to the nearest survey plot border. Conversely, 25% of all trees cataloged in the manual survey plots were, on average, located 5.57 m or less from the closest boundary of the respective survey plot. On a theoretical plot, where all trees would be distributed absolutely evenly, 25% of the trees would be located at a distance of 3.43 m from the plot boundary (Fig. 3).

Following repeated inventories using the same measurement methods on identical plots, the precision of determining tree stem locations was found to be higher with TLS than with CMM. Trees measured repeatedly with TLS exhibited an average error of 0.16 m ($\sigma = 0.08$ m), while CMM demonstrated an average error of 3.9 m ($\sigma = 2.06$ m) (Table 3).

To examine the potential for error propagation in tree position measurements during CMM, we conducted a test to determine the correlation between differences in stem location and their distance to the boundary of the survey plot. Results demonstrated a slightly positive, statistically significant correlation on plot H ($r = 0.119$, $p = 0.014$), suggesting that during CMM, the discrepancies in repeated stem position measurements increased slightly with proximity to the plot border. For plot N, the correlation was more pronounced ($r = 0.311$) and highly significant

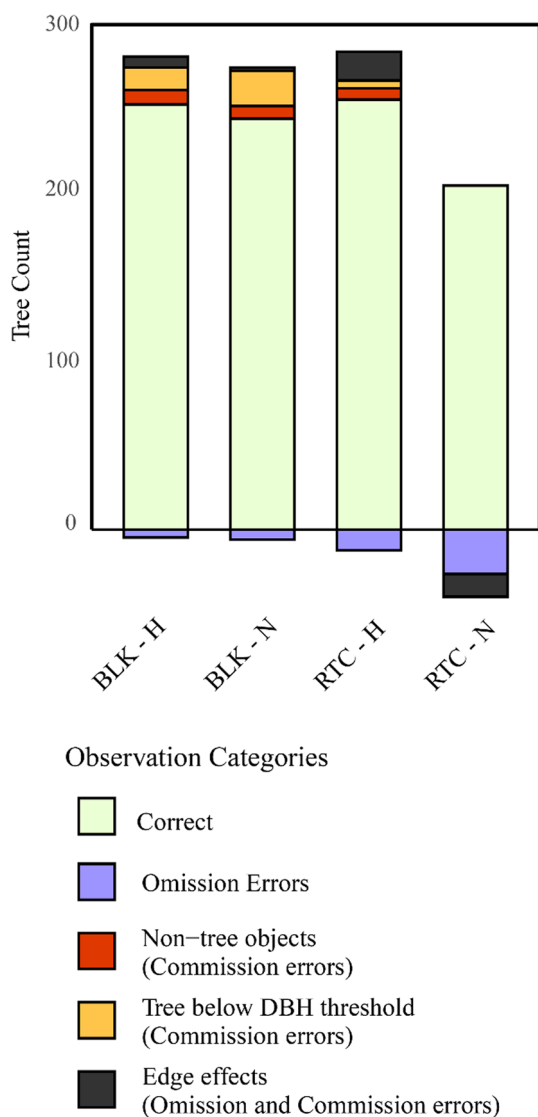


Fig. 1 Number of trees automatically detected using TLS for both the BLK and the RTC models across different plots (“H” and “N”). The data are segmented into correctly identified trees and various error types. Negative bars indicate trees omitted from the dataset

($p < 0.001$), indicating a stronger potential for measurement errors in tree positions with respect to the distance from the edge of the plots.

Single-tree parameters: tree DBH, height, and volume

DBH estimations from automated TLS closely align with those observed in CMM, with a root-mean-square error (RMSE) of 0.04 m and an average error of 0.01 m. Notably, there are a few outliers that overestimate the manually measured DBH by 0.1–0.2 m (Fig. 4 a). For tree height estimations using TLS, a distinctly negative trend is observed

Table 2 Descriptive statistics on the distribution of tree detection outcomes for different plots and employed TLS models

	BLK		RTC		Mean
	H	N	H	N	
Correct	267	258	270	216	253
Omission error	5	7	13	28	13
Commission error (Non-Tree)	9	8	7	0	6
Commission error (Tree)	14	22	5	0	10
Edge effect	7	2	18	14	10

Trees of a low DBH under the 0.07 m threshold which have been included in the analysis data due to an overestimation of their DBH are listed under “Commission Error (Tree).” All other false positive tree detections are listed as “Commission Error (Non-Tree)”

compared to CMM as tree height increases. While deviations from CMM for tree heights below 20 m are relatively small, with an RMSE of 2.03 m and a mean error of 0.03 m, they shift to a significantly negative range for tree heights above 30 m, with an RMSE of 5.6 m and a mean error of -4.53 m. Consequently, the heights of taller trees are substantially underestimated by automated TLS measurements, with extreme values up to -10 m, whereas the heights of shorter trees are estimated more accurately (Fig. 4a). The automated TLS estimations of DBH from the Leica BLK360 were, on average, 0.01 m lower than those of the RTC360 ($p = 0.013$). Furthermore, tree heights estimated by the BLK360 were 0.62 m lower than by the RTC360 ($p = 0.09$), as detailed in Table 4.

When examining the height–diameter relationship across different tree measurement techniques, the measurement techniques follow the order of semi-automated TLS (RSS = 433.2), CMM (RSS = 495.9), to automated TLS (RSS = 910.6) in terms of variability, with the automated TLS demonstrating a higher RSS value. However, according to the Wilcoxon rank sum test, these differences were statistically not significant (p values > 0.05). Despite TLS’s higher mean deviation and RSS, the relationship between tree height and DBH remained consistent, evidenced by the stable coefficients in our model (Regression curve proposed by Prodan 2014), $a_0 = 0.0004$, $a_1 = 0.0099$, $a_2 = 0.0171$), indicating dependable predictions (Fig. 5).

Plenter structure and stand parameters

Each measurement method successfully illustrated the distinctive curve characteristic of a plenter forest, revealing not only its general shape, but also the nuanced variations within the curve (Fig. 6). However, automatic TLS measurements assigned less trees into small DBH classes compared to CMM. In the CMM inventories from 2018 and 2022, 43.2 and 39.3% of the measured trees exhibited a DBH smaller

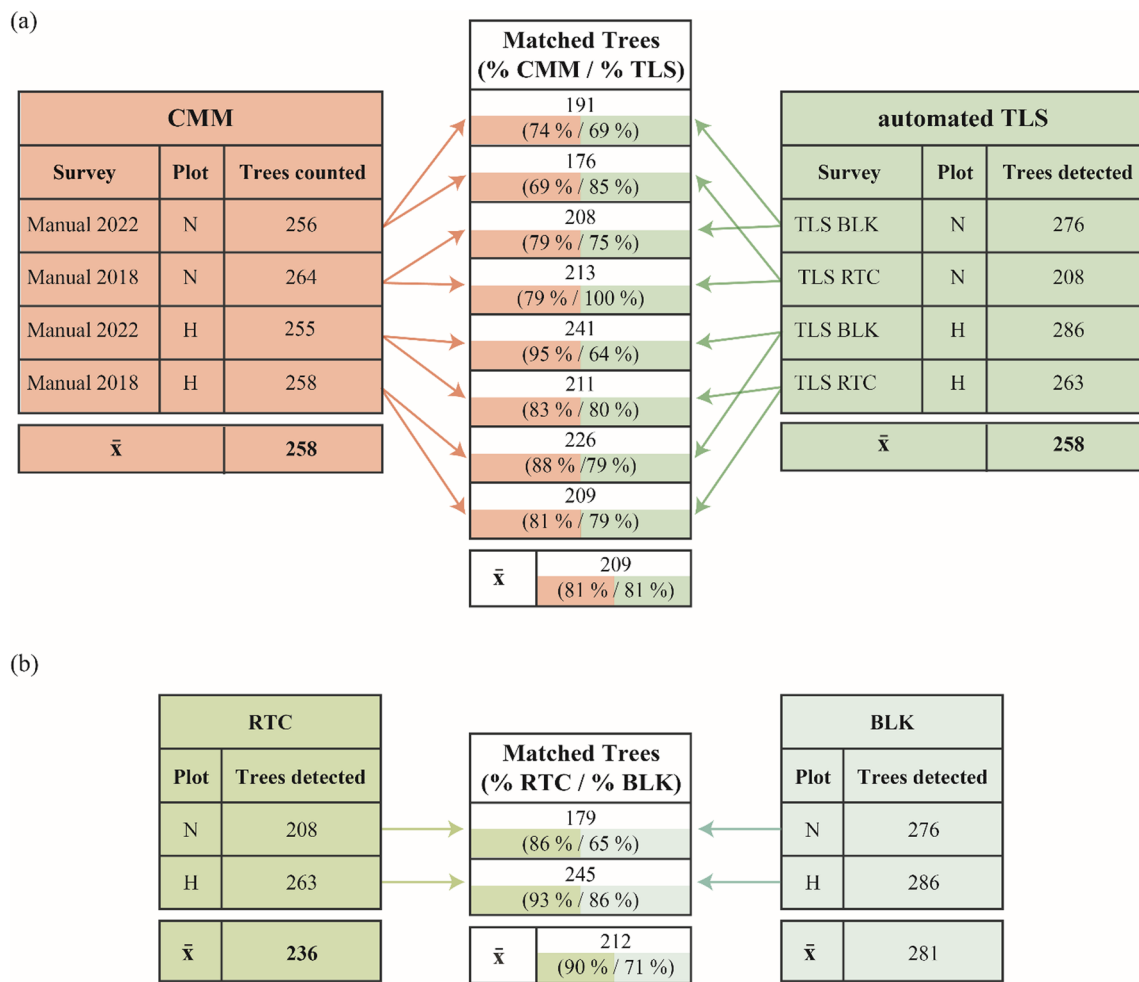


Fig. 2 Automatically matched trees between CMM and automated TLS (a) and between the two different TLS models, RTC and BLK (b)

than 0.15 m, respectively. In contrast, surveys using automated TLS detected a lower proportion of trees with DBH < 0.15 m: BLK—34.1%, RTC—35.5%. Conversely, medium-diameter trees were detected more frequently using TLS, where 36.9% of trees identified by the BLK and 40.7% by the RTC models had a DBH between 0.2 and 0.54 m. These findings contrast with the CMM surveys conducted in 2018 and 2022, which reported 31.6 and 32.5% of trees within this DBH range, respectively. The discrepancies in DBH distribution between the two measurement methods are smaller for trees with larger DBH. For trees with a DBH greater than 0.55 m, the percentages recorded by CMM in 2018 and 2022 were 11.3 and 10.1%. Meanwhile, automated TLS measurements with the BLK and RTC registered 9.7 and 10.2% of trees within this DBH range (Fig. 6). The CMM and automated TLS measurement techniques were compared for differences in tree stem counting, basal area, and standing wood volume estimation. CMM found an average of 516 tree stems per hectare, slightly fewer than the 523 tree stems per hectare detected by TLS, which showed varying results. The RTC TLS showed a

tendency to underestimate the basal area by 7.7 and 4.5% when compared to the 2018 and 2022 CMM inventories. In contrast, the BLK overestimated the basal area by 7.7 and 14.4% for the same periods. Regarding standing wood volume, average CMM estimates outpaced RTC and BLK TLS estimates by an average of 23.3 and 3.9%, respectively. Differences in mean DBH, mean tree height, and top tree height followed similar trends to those observed at the individual tree level (Fig. 4), with the mean DBH being on average 0.012 m higher when measured using automated TLS. Tree heights were underestimated by automated TLS, with a mean underestimation of 1.6 m for mean tree height and a larger underestimation of 4.1 m for the top tree height (Table 5).

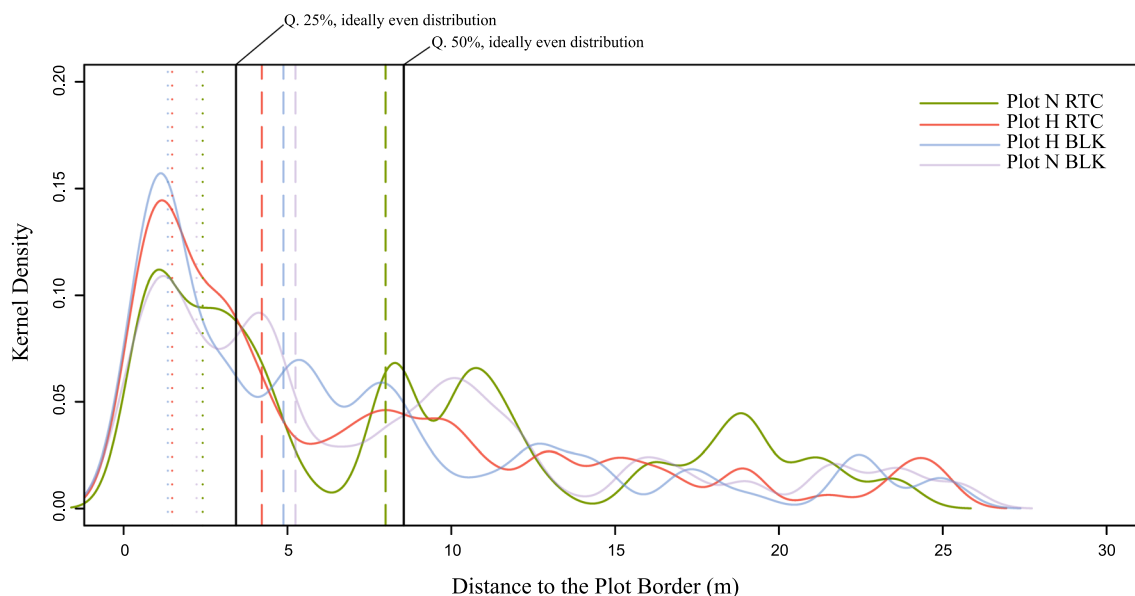


Fig. 3 Distance of unmatched remaining trees, from PCD measured by automated TLS, to the closest survey plot border. Dotted and dashed vertical lines represent the first (25%) and second (50%) quan-

tile of all trees closest to the plot border for Plot N and Plot H for both BLK and RTC. Solid vertical lines are added as a reference for an ideally even distribution of trees on a theoretical plot

Table 3 Average deviation and standard deviation (SD) of tree positions after being measured repeatedly for both CMM and automated TLS

Methods	Plots	Mean position deviation (m)		SD (m)	
Automated TLS	H	0.077	0.155	0.139	0.084
	N	0.239		0.068	
CMM	H	3.387	3.902	2.102	2.059
	N	4.552		2.017	

Discussion

Automated tree mapping for long-term monitoring plots

Automated tree detection

Most commission errors identified using the BLK model were attributable to trees below the DBH threshold of 0.07 m that were wrongfully included in the dataset due to overestimation of their DBH. Equivalently, Bienert et al. (2018) noted a tenfold increase in overall commission errors, constituting 57% of detected trees in a plot resembling the structure of a plenter forest, largely attributing it to a high density of young understory trees. Commission errors of this type could be facilitated, among other factors, by the high density of branches present at the DBH measurement point of 1.3 m, particularly in young trees

found within the survey plots. Frequently, these trees are situated within dense vegetation cones, further complicating an accurate measurement of the DBH. This error type was more prominent with the lower-end BLK model, where stronger noise within the PCD could have contributed significantly to the error, exerting a greater effect on trees with lower DBH. Another significant category of tree detection errors stemmed from edge effects. In three out of four instances, trees were erroneously incorporated from areas outside the specified survey plots, and in one instance, trees from within the survey plot were mistakenly positioned outside of it. This introduces an additional error source that is less influenced by forest structural attributes, such as tree density, or the intrinsic qualities of the PCD, which encompass point density, noise, and tree stem completeness. Instead, it is mainly attributed to inaccuracies in defining the boundaries of the test area and potentially due to variations in the precision of scan co-registration within the PCD. Another manifestation of edge effects, which entails shifts in PCD quality, could be the increased error rates in tree detection toward the plot's edge, as noted by Ritter et al. (2017). In this study, both commission and omission errors escalated with a reduction in the buffer size surrounding their survey area. Consequently, both tree detection errors with origins in PCD quality and those without may have influenced the trend of an increasing number of unmatched trees observed in our study (Fig. 3). A crucial factor that might influence the rate of successful tree detections is the forest structure, particularly since plenter forests

Fig. 4 DBH and tree height deviations between automated TLS and CMM (a) and between automated TLS- and semi-automated TLS measurements (b). The red dashed line is the CMM as reference measurement. The solid blue line shows the estimated relationship between the x and y variables, based on the locally weighted running line smoother (loess) method with a span parameter of 0.5. The gray shaded area represents the 95% confidence interval around this estimate

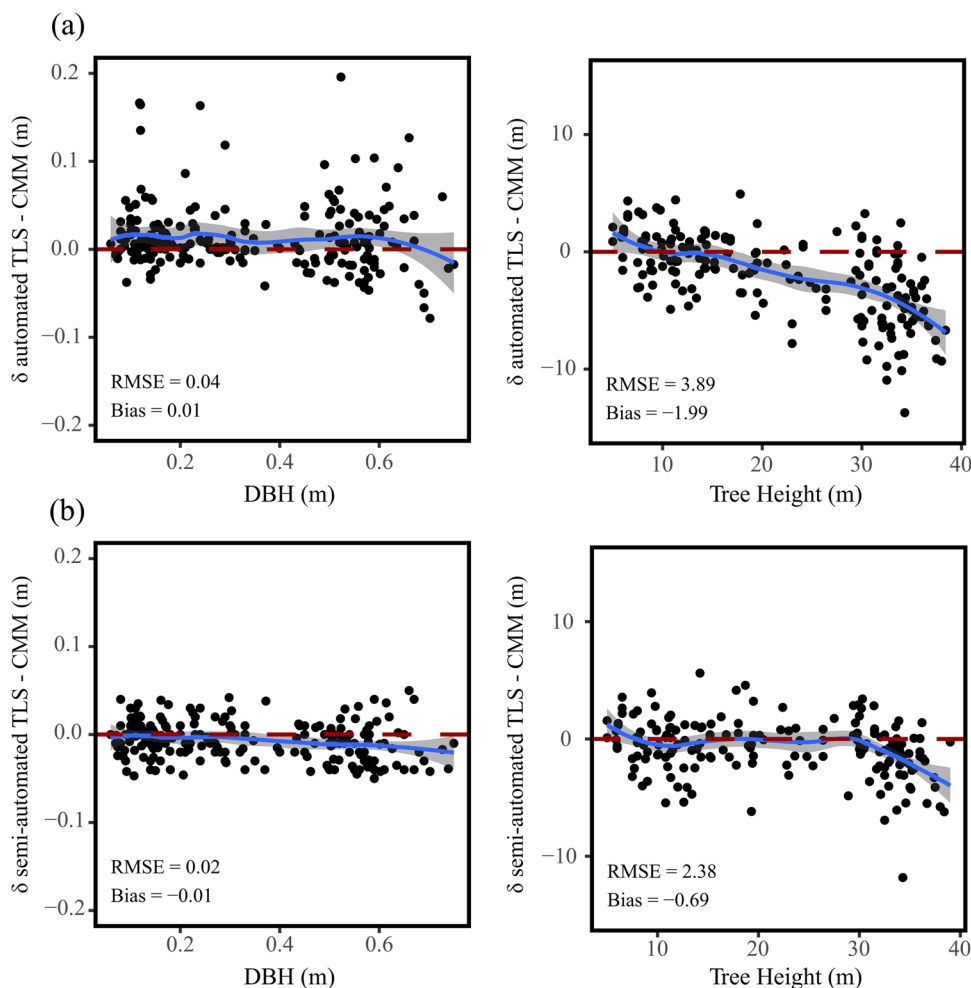


Table 4 Differences between tree metrics of automated TLS and CMM measurements for different TLS systems (BLK=Leica BLK360, RTC=Leica RTC360) and between the two different TLS systems

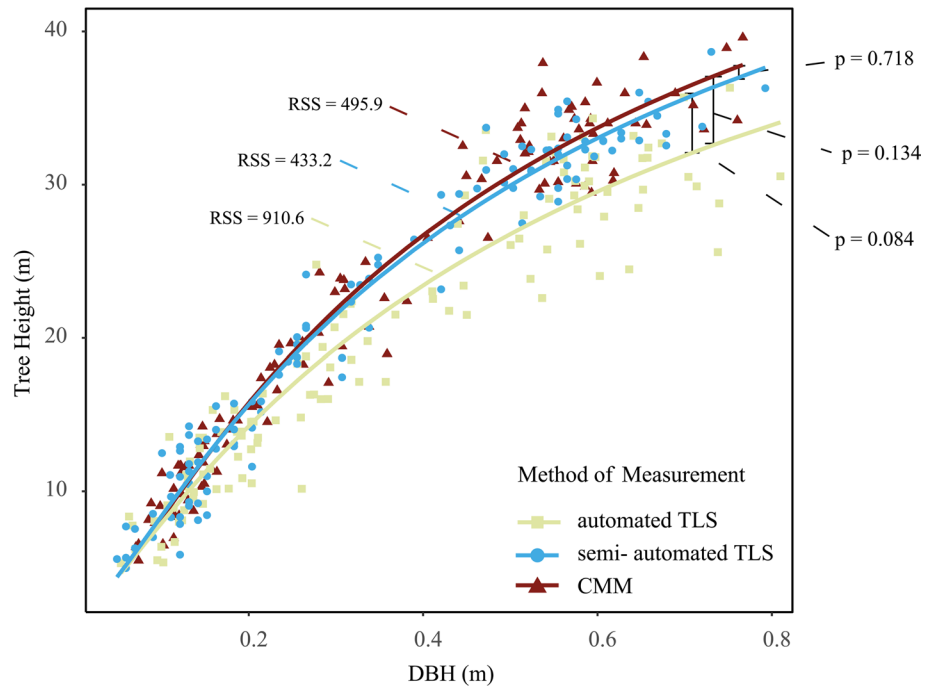
TLS system and measurement method	Tree height		DBH	
	p value	Mean difference (m)	p value	Mean difference (m)
RTC automated TLS–CMM	<0.001	-1.72	<0.001	0.015
BLK automated TLS–CMM	0.006	-2.33	<0.001	0.012
BLK automated TLS–RTC automated TLS	0.09	-0.62	0.013	-0.01

p values were calculated using the Wilcoxon rank sum test

are characterized by their unique structure, marked by a high proportion of trees with small diameters. Previous research has indicated that dense forests with a considerable presence of understory trees frequently lead to undetected tree locations. A study conducted by Gollob et al. (2019) investigated the effects of the number and distance of scan positions on tree detection rates in TLS surveys. Employing a rectangular grid with a 10-m edge length, they noted tree detection rates fluctuating between 66.6% (DBH ≥ 0.05 m) and 83.5% (DBH ≥ 0.15 m). These data suggest that trees within the lower DBH classes are

more prone to being overlooked, a situation that resonates with the predominant tree population in the plenter forest survey plots. Despite the significant presence of trees with lower DBHs in our study, highlighted by a median DBH of only 0.17 m, the number of accurately identified trees and the associated error magnitudes (composed of omission and commission errors) largely align with the outcomes of similar studies. Yang et al. (2016) reported average commission and omission error rates of 10.8 and 12.9%, respectively, whereas Ritter et al. (2017) documented lower error rates of 2.7 and 5.7% for omission

Fig. 5 Scatter plot between DBH and tree height for CMM, automated TLS, and semi-automated TLS. *P* values of a Wilcoxon rank sum test with continuity correction for predicted tree height based on the applied multiple regression mode and residual sum-of-squares (RSS) of model fitting



and commission errors, respectively. It is worth noting that both cited studies were executed in stands with fewer understory trees compared to the plenter forest plots investigated in our study.

Automated tree mapping

The average distances between pairs of matched tree positions, when manually measured, were found to be twenty-six times greater than those measured by automated TLS. This suggests a relatively high precision in determining tree locations from PCD. In a benchmarking project conducted by Liang et al. (2018), a similar automated tree-matching method was employed, utilizing tree location and DBH as primary matching parameters. Match-finding iterations were repeated based on duplicates and unmatched trees. They reported RMSE values for stem locations ranging from 5 cm in “easy” complexity plots to 10 cm in “difficult” ones. The structural appearance and DBH class distribution of their “difficult” category share similarities with the plenter forest. In the medium complexity plots, Liang et al. (2018) achieved a match between trees in 88% of cases, while in difficult complexity plots, the match rate was 66.2%. Similarly, our study demonstrated an 81% match rate for manually measured reference trees with automatically TLS-derived trees, and match rates of 87 and 74% between repeated automated TLS measurements.

Limitations in assessing automated tree detection and mapping

Unlike in the studies carried out by Liang et al. (2018) and Ritter et al. (2017), our study design did not incorporate a dedicated measure to ascertain the precision of automated tree pairing, which could potentially impact the reliability of our findings. Moreover, the irregular structures observed in the plenter forest stands might have resulted in varying distances between scanner locations. This variation could have led to inhomogeneous point densities across the study area. Although high peaks of local point densities were mitigated by voxelization, areas of particularly low-point densities remained, possibly increasing the chance of omission errors. This might have been particularly evident with plot N, which exhibited the highest frequency of omission errors. The omission of 28 trees in a single plot might have been exacerbated by a missing scan in the scanner position grid, resulting in a 20×20 m area within the PCD devoid of any TLS deployment. Lastly, the analysis revealed divergent patterns in the omission and commission error ratios between the different models utilized.

Single-tree parameters

Tree height estimation

Our study revealed a tendency toward underestimation of tree height in automated TLS measurements. This underestimation becomes particularly noticeable for trees above

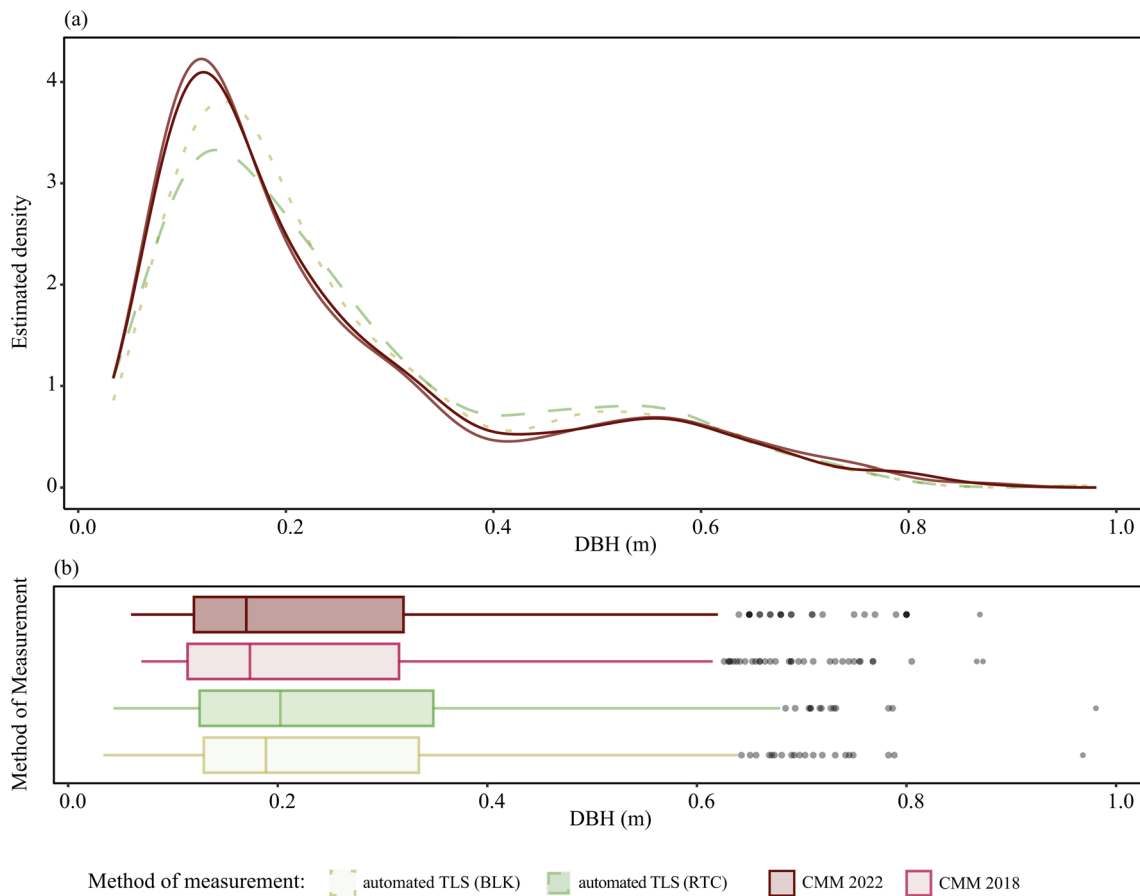


Fig. 6 Distribution of DBH for different measurement methods. **a** Kernel density estimation distribution of DBH for different measurement methods. The smooth curves represent the estimated probability density function of the DBH for each method: TLS measurements using the BLK model (“automated TLS (BLK),” $n = 568$), TLS measurements using the RTC model (“automated TLS (RTC),” $n = 486$), CMM from a survey in 2018 (“CMM 2018,” $n = 522$) and CMM from a survey in 2022 (“CMM 2022,” $n = 510$). **b** Boxplots for all DBH measurement methods, including outliers and a 95% confidence interval for the median

Table 5 Comparison of key forest management metrics between automated TLS and CMM measurement methods and their respective surveys. Means are calculated as the average of the two respective surveys

Survey method	Trees per ha	Basal area ($m^2 \times ha^{-1}$)	Standing wood volume ($m^3 \times ha^{-1}$)	Mean tree height (m)	Mean DBH (m)	Top tree height (m)
Automated TLS						
Survey using RTC360	479.0	35.9	407.5	15.9	0.255	28.9
Survey using BLK360	567.0	41.9	473.5	15.2	0.261	28.9
Mean	523.0	38.9	440.5	15.5	0.258	28.6
Mean error	44.0	3.0	34.5	1.99	0.029	0.51
CMM						
Manual survey (2018)	522.0	38.9	502.1	17.1	0.246	32.9
Manual survey (2022)	510.0	37.6	483.2	17.1	0.247	32.7
Mean	516.0	38.2	492.7	17.1	0.246	32.8
Mean error	6.0	0.7	0.8	*	0.028	*

The mean error evaluates the consistency of measurements between two surveys for the same plots. This is achieved by calculating the average difference in measurements for each plot across the two surveys

*Mean height and top tree height error for CMM cannot be calculated because no separate measurements of tree height were conducted for the 2022 inventory

the third quantile when sorted by volume. Notably, a bias of -4.53 m was observed for trees over 30 m in height, as measured automatically by TLS. This error is likely attributed to a decrease in PCD density at higher elevations, leading to individual points at those heights being unrecognized as part of the targeted tree. The presence of an overall negative bias in tree height estimation is a common phenomenon reported in various studies. This bias has been observed using diverse methods in a benchmarking study by Liang et al. (2018), the application of a voxel-based region growing crown segmentation algorithm by Tockner et al. (2022) and 3D cylinder fitting, as described by Moskal et al. (2011).

Tree DBH estimation

When comparing automated TLS to CMM and semi-automated TLS measurements, it was found that the estimations of DBH for trees exhibited a slight positive bias. The sources of bias in DBH estimates derived from TLS measurements can vary and result in either underestimation or overestimation of tree DBH. Common errors can arise from occlusion effects on the stem cross-section or difficulties in accurately separating stem cross-sections from attached branches or nearby vegetation. In this study, the latter source of error may have had a more significant impact than occlusion effects. Previous studies have reported that increased noise in TLS data can lead to a positive bias in DBH estimations, particularly for small trees with a DBH less than 10 cm (Gollob et al. 2020), as well as in plots with dense vegetation (Liang et al. 2018). These factors are likely to contribute to the observed slight positive bias in DBH estimations from automated TLS measurements in our study.

Key metrics of plenter forest management

The DBH distribution within the forest stand exhibits a characteristic “reverse-J-shaped” curve, typical for a plenter forest. This pattern remains consistent regardless of whether the trees are measured with TLS or by CMM, highlighting features such as the noticeable indentation within the 40-cm DBH class range, which is present in all measurements. The omission of small-dimension trees in automated TLS measurements is likely due to overlooked trees. This suggests that automated TLS measurements are effective in capturing the structural characteristics of a plenter forest, essential for planning future harvest operations to sustain the equilibrium state of the plenter forest structure. For foresters and forest owners, growing stock is a standard metric for timing harvest operations and assessing volume. In our study, basal area was found to be a more reliable indicator of growing stock compared to standing wood volume. Both basal area and standing wood volume are subject to errors in tree detection. However, the notable underestimation of tree

height by automated TLS particularly affects standing wood volume measurements. Similarly, the top tree height, another metric based on individual tree height in forest stands, is adversely affected by this underestimation. This error in tree height measurement by automated TLS could lead to the underestimation of the forest stand’s site index.

TLS device-related differences in measurements

The TLS devices used in this study are from different price ranges, with the Leica RTC360 being the higher-end model compared to the Leica BLK360. The RTC model offers improved technical specifications, which could potentially enhance measurement results and precision. The BLK model’s maximum range of 60 m is notably shorter than the RTC’s range of 130 m, which might imply a disadvantage in tree height measurements. However, differences in height measurements between the devices were not statistically significant, with the BLK showing a slight negative bias. The dense grid of TLS placements seemed to mitigate the BLK’s shorter range. In terms of DBH estimation, differences were minor at 0.01 m but still statistically significant. Despite the RTC’s higher 3D point accuracy, the results indicated lower accuracy for this model when considering CMM measurements as the gold standard. It is crucial, however, to consider additional factors that could have influenced these estimations, such as the precision of individual TLS scan registrations, the positioning and number of scanner placements within the forest plot, which could introduce user error, and TLS calibration. Given that the study was conducted on only two research plots, the influence of the previously mentioned error factors might have masked any inaccuracies attributable to the technical specifications of the TLS models used.

Future prospects for TLS applications in complex forests

Our experience indicates that using TLS reduces forest measurement time compared to manual methods, albeit requiring additional post-processing of the PCD. However, further optimization of the scanning process is possible by employing mobile technologies such as unmanned aerial vehicles (UAVs) or personal laser scanning systems (PLS) equipped with simultaneous localizations and mapping (SLAM) technology. Approaches using PLS not only prove to be time-efficient, but also hold promising advantages in tree- and plot-level estimates, as reported by Gollob et al. (2020) and Bauwens et al. (2016). Gollob et al. (2020) reported that the scanning process of a plot was completed 4.7 times faster with PLS and SLAM than with a TLS. PLS also improved tree detection rates to 96%, compared to TLS’s 78.5%, mainly due to reduced occlusion effects.

Bauwens et al. (2016) compared the stem cross-section closure at 1.3 m height, finding a complete closure for 91% of trees using PLS, compared to 42% using TLS, but reported limitations of PLS in capturing tree canopies beyond 15–20 m. Limitations in scanning the tree canopy were also found in our study, despite the application of TLS. Enhanced coverage of the forest canopy can be achieved by combining UAV and TLS data, although it is more time-consuming (Donager et al. 2018; Terryn et al. 2022; Brede et al. 2017; Tian et al. 2019). While enhancing forest canopy coverage could indeed improve height estimates and subsequently volume predictions via allometric models, it is possible to measure tree volume directly, bypassing potential errors in DBH and height estimations. An additional challenge with allometric models is that some require tree species as an input parameter. Though there exist methods employing UAV multispectral ortho-images to identify tree species (Kampen et al. 2019; Feng et al. 2019), they could potentially compromise efficiency. More direct and practical approaches for estimating tree volume include voxel-based methods, cylinder fitting, and quantitative structure models (Bienert et al. 2014; Raunonen et al. 2013; An and Froese 2023). Furthermore, it is important to explore the capabilities of laser scanning beyond duplicating measurements gathered by CMM. Developing techniques to extract relevant information from PCD for stand description can offer new opportunities to refine standard inventory practices. Studies from recent years have examined the potential of 3D point cloud data for characterizing forest structure and complexity, including techniques to quantify individual tree complexity using fractal analysis (Seidel 2018), evaluate the influence of tree characteristics on forest complexity (Seidel et al. 2019) and develop indices for stand structural complexity linked to biodiversity and ecosystem functioning (Ehbrecht et al. 2017). Stiers et al. (2020) developed a scaled index that describes the ideal structure specifically of a CFF and compared it with even-aged forest stands. Approaches like this could enable novel methods to quantify differences between the current state of a CCF stand structure and an ideal target structure, thereby guiding forest management operations more effectively.

Conclusion

In this study, we evaluated the use of TLS for long-term monitoring in a complex, highly structured and dense plenter forest. Our research has shown promising results, particularly in the accuracy of estimated single-tree parameters, DBH and tree height, and also yielding satisfactory accuracy for tree volume estimation. Stand-level parameters, such as stand volume and basal area, showed

minor discrepancies primarily due to edge effect errors in tree detection. However, given the challenging conditions of conducting such a study in a densely structured forest, the tree detection rate was found to be adequate when compared to similar studies. Although some inaccuracies were observed, these do not undermine the potential of automated measurements like TLS for conducting precise forest inventories. We suggest enhancements, such as refining methodological approaches for tree detection and improving estimation of single tree parameters. In order to minimize commission errors in areas with dense understory vegetation, a denser rectangular measurement grid smaller than 10×10 m employing should be considered. According to previous studies, utilizing PLS systems holds promise for reducing both the omission of automatically detected trees and discrepancies in tree height and volume estimations. However, inaccuracies in individual tree measurements were not solely a result of gaps in the PCD, but also stemmed from the inadequate harnessing of the available data through current algorithms. Hence, the development and implementation of more refined algorithms may facilitate the utilization of the PCD, thereby enhancing the accuracy of the outcomes. Adoption of automated methods such as TLS could be viable in complex forest structures like plenter and conversion or restoration forests, leading to more accurate and efficient inventories, followed by optimized strategies for sustainable forest management.

Acknowledgements We thank the “Waldbau und Bergwald”- department of the Bavarian State Institute of Forestry (LWF) and its head, Dr. Hans-Joachim Klemmt, for generously lending us the Leica BLK360 terrestrial laser scanner for our field survey. We thank Lisa Irrgang, Anton Schloer and Till Schmid-Lameck for their indispensable contribution to the field work.

Author contributions All authors contributed to the study conception and design. Material preparation, data collection and analysis were performed by YW. The first draft of the manuscript was written by YW, and all authors commented on previous versions of the manuscript. All authors read and approved the final manuscript.

Funding Open Access funding enabled and organized by Projekt DEAL. This work was supported by the German Federal Ministry of Food and Agriculture & Federal Office for Agriculture and Food within the German–Japanese project “3Arrows” under the Grant (28I-038-01). The article processing charge was funded by the Baden-Württemberg Ministry of Science, Research and Culture and the University of Applied Forest Sciences Rottenburg in the funding program Open Access Publishing.

Data availability Data will be made available upon request.

Code availability Code will be made available upon request.

Declarations

Competing interests The authors declare no competing interests.

Open Access This article is licensed under a Creative Commons Attribution 4.0 International License, which permits use, sharing, adaptation, distribution and reproduction in any medium or format, as long as you give appropriate credit to the original author(s) and the source, provide a link to the Creative Commons licence, and indicate if changes were made. The images or other third party material in this article are included in the article's Creative Commons licence, unless indicated otherwise in a credit line to the material. If material is not included in the article's Creative Commons licence and your intended use is not permitted by statutory regulation or exceeds the permitted use, you will need to obtain permission directly from the copyright holder. To view a copy of this licence, visit <http://creativecommons.org/licenses/by/4.0/>.

References

- An Z, Froese RE (2023) Tree stem volume estimation from terrestrial LiDAR point cloud by unwrapping. *Can J for Res* 53(2):60–70. <https://doi.org/10.1139/cjfr-2022-0153>
- Ankerst M et al (1999) OPTICS: ordering points to identify the clustering structure. *ACM SIGMOD Rec* 28(2):49–60. <https://doi.org/10.1145/304181.304187>
- Bartsch N, von Lupke B, Rohrig E (2020) *Waldbau auf oekologischer Grundlage. 8., vollstaendig ueberarbeitete und erweiterte Auflage*. Stuttgart: Verlag Eugen Ulmer (UTB Forstwissenschaften, Agrarwissenschaften, Oekologie, Biologie, 8310)
- Bauwens S et al (2016) Forest inventory with terrestrial LiDAR: a comparison of static and hand-held mobile laser scanning. *Forests* 7(12):127. <https://doi.org/10.3390/f7060127>
- Besl PJ, McKay ND (1992) A method for registration of 3-D shapes. *IEEE Trans Pattern Anal Mach Intell* 14(2):239–256. <https://doi.org/10.1109/34.121791>
- Bienert A et al (2014) A voxel-based technique to estimate the volume of trees from terrestrial laser scanner data. *Int Arch Photogramm Remote Sens Spat Inf Sci* 40:101–106
- Bienert A et al (2018) Comparison and combination of mobile and terrestrial laser scanning for natural forest inventories. *Forests* 9(7):395. <https://doi.org/10.3390/f9070395>
- Brede B et al (2017) Comparing RIEGL RiCOPTER UAV LiDAR derived canopy height and DBH with terrestrial LiDAR. *Sensors* 17(10):2371. <https://doi.org/10.3390/s17102371>
- Calders K et al (2020) Terrestrial laser scanning in forest ecology: Expanding the horizon. *Remote Sens Environ* 251:112102. <https://doi.org/10.1016/j.rse.2020.112102>
- Dannecker K (1955) *Aus der hohen Schule des Weißtannenwaldes*. Sauerlaender Verlag, Frankfurt am Main
- Díaz-Yáñez O et al (2017) How does forest composition and structure affect the stability against wind and snow? *For Ecol Manag* 401:215–222. <https://doi.org/10.1016/j.foreco.2017.06.054>
- CloudCompare Team (2020) *CloudCompare (Version 2.11.3)* [Computer software]. www.danielgm.net/cc/
- Donager JJ et al (2018) Examining forest structure with terrestrial lidar: suggestions and novel techniques based on comparisons between scanners and forest treatments. *Earth Space Sci* 5(11):753–776. <https://doi.org/10.1029/2018EA000417>
- Dvorak L (2000) *Kontrollstichproben im Plenterwald* [application/pdf]. ETH Zurich. <https://doi.org/10.3929/ETHZ-A-004145901>
- Ehbrecht M et al (2017) Quantifying stand structural complexity and its relationship with forest management, tree species diversity and microclimate. *Agric for Meteorol* 242:1–9. <https://doi.org/10.1016/j.agrformet.2017.04.012>
- Ester M et al (1996) A density-based algorithm for discovering clusters in large spatial databases with noise. In: (KDD-96) proceedings, pp 226–231
- Feng X, Li P (2019) A tree species mapping method from UAV images over urban area using similarity in tree-crown object histograms. *Remote Sens* 11(17):1982. <https://doi.org/10.3390/rs11171982>
- Fick SE, Hijmans RJ (2017) WorldClim 2: new 1km spatial resolution climate surfaces for global land areas. *Int J Climatol* 37(12):4302–4315
- Gollob C et al (2019) Influence of scanner position and plot size on the accuracy of tree detection and diameter estimation using terrestrial laser scanning on forest inventory plots. *Remote Sens* 11(13):1602. <https://doi.org/10.3390/rs11131602>
- Gollob C, Ritter T, Nothdurft A (2020) Forest inventory with long range and high-speed personal laser scanning (PLS) and simultaneous localization and mapping (SLAM) technology. *Remote Sens* 12(9):1509. <https://doi.org/10.3390/rs12091509>
- Hopkinson C et al (2004) Assessing forest metrics with a ground-based scanning lidar. *Can J for Res* 34(3):573–583. <https://doi.org/10.1139/x03-225>
- Kampen M et al (2019) UAV-based multispectral data for tree species classification and tree vitality analysis. *Dreilaendertagung der DGPF, der OVG und der SGPF in Wien, Oesterreich*
- Knoke T (1998) *Analyse und Optimierung der Holzproduktion in einem Plenterwald: zur Forstbetriebsplanung in ungleichaltrigen Wäldern*. Frank (Forstliche Forschungsberichte München), München, p 170
- Kublin E (2003) *Einheitliche Beschreibung der Schaftform—Methoden und Programme—BDATPro. A uniform description of stem profiles—methods and programs—BDATPro*. *Forstwiss Centralbl* 122(3):183–200. <https://doi.org/10.1046/j.1439-0337.2003.00183.x>
- Kurth A (1954) Die Kontrollidee in der schweizerischen Forstwirtschaft. *AFJZ* 125:4
- Lenk E, Kenk G (2007) *Sortenproduktion und Risiken Schwarzwälder Plenterwälder*. *AFZ DerWald* 3:132–135
- Liang X et al (2016) Terrestrial laser scanning in forest inventories. *ISPRS J Photogramm Remote Sens* 115:63–77. <https://doi.org/10.1016/j.isprsjprs.2016.01.006>
- Liang X et al (2018) International benchmarking of terrestrial laser scanning approaches for forest inventories. *ISPRS J Photogramm Remote Sens* 144:137–179. <https://doi.org/10.1016/j.isprsjprs.2018.06.021>
- Lovell JL et al (2003) Using airborne and ground-based ranging lidar to measure canopy structure in Australian forests. *Can J Remote Sens* 29(5):607–622. <https://doi.org/10.5589/m03-026>
- Mason WL, Diaci J, Carvalho J, Valkonen S (2022) Continuous cover forestry in Europe: usage and the knowledge gaps and challenges to wider adoption. *Forestry: An Int J For Res* 95:1–12. <https://doi.org/10.1093/forestry/cpab038>
- Moskal LM, Zheng G (2011) Retrieving forest inventory variables with terrestrial laser scanning (TLS) in urban heterogeneous forest. *Remote Sens* 4(1):1–20. <https://doi.org/10.3390/rs4010001>
- O'Hara K, Hasenauer H, Kindermann G (2007) Sustainability in multi-aged stands: an analysis of long-term plenter systems. *Forestry* 80:163–181
- Pretzsch H (2009) *Forest dynamics, growth and yield: from measurement to model*. Springer, Berlin
- Prodan M (2014) *Forstliche biometrie*. Reprint der Ausg. BLV-Verl., Muenchen, 1961. Kessel, Remagen-Oberwinter
- R Core Team (2023) *R: a language and environment for statistical computing*. R Foundation for Statistical Computing, Vienna, Austria. <https://www.R-project.org/>
- Raunonen P et al (2013) Fast automatic precision tree models from terrestrial laser scanner data. *Remote Sens* 5(2):491–520. <https://doi.org/10.3390/rs5020491>
- Ritter T et al (2017) Automatic mapping of forest stands based on three-dimensional point clouds derived from terrestrial laser-scanning. *Forests* 8(8):265. <https://doi.org/10.3390/f8080265>

- Roussel J, Auty D, Coops NC, Tompalski P, Goodbody TR, Meador AS, Bourdon J, de Boissieu F, Achim A (2020) lidR: an R package for analysis of Airborne Laser Scanning (ALS) data. *Remote Sens Environ* 251:112061. <https://doi.org/10.1016/j.rse.2020.112061>
- Schuetz JP (2001) Plenter-forests and other types of structured and mixed forests. Paul Parey, Berlin (**in German**)
- Seidel D (2018) A holistic approach to determine tree structural complexity based on laser scanning data and fractal analysis. *Ecol Evol* 8(1):128–134. <https://doi.org/10.1002/ece3.3661>
- Seidel D, Ammer C (2023) Towards a causal understanding of the relationship between structural complexity, productivity, and adaptability of forests based on principles of thermodynamics. *For Ecol Manag* 544:121238. <https://doi.org/10.1016/j.foreco.2023.121238>
- Seidel D et al (2019) From tree to stand-level structural complexity—Which properties make a forest stand complex? *Agric for Meteorol* 278:107699. <https://doi.org/10.1016/j.agrformet.2019.107699>
- Stiers M et al (2020) Quantifying the target state of forest stands managed with the continuous cover approach—revisiting Möller’s “Dauerwald” concept after 100 years. *Trees for People* 1:100004. <https://doi.org/10.1016/j.tfp.2020.100004>
- Terryn L et al (2022) Quantifying tropical forest structure through terrestrial and UAV laser scanning fusion in Australian rainforests. *Remote Sens Environ* 271:112912. <https://doi.org/10.1016/j.rse.2022.112912>
- Tian J et al (2019) A novel tree height extraction approach for individual trees by combining TLS and UAV image-based point cloud integration. *Forests* 10(7):537. <https://doi.org/10.3390/f10070537>
- Tockner A et al (2022) Automatic tree crown segmentation using dense forest point clouds from Personal Laser Scanning (PLS). *Int J Appl Earth Obs Geoinf* 114:103025. <https://doi.org/10.1016/j.jag.2022.103025>
- Yang B et al (2016) Automatic forest mapping at individual tree levels from terrestrial laser scanning point clouds with a hierarchical minimum cut method. *Remote Sens* 8(5):372. <https://doi.org/10.3390/rs8050372>
- Zingg A et al (2009) ‘Ertragskundliche Leistung in den Plenterwald-Versuchsflaechen der Schweiz | Yield performance in the plenter forest research plots in Switzerland. *Schweiz Z Forstwes* 160(6):162–174. <https://doi.org/10.3188/szf.2009.0162>

Publisher's Note Springer Nature remains neutral with regard to jurisdictional claims in published maps and institutional affiliations.